THE JOURNAL OF PHYSICAL CHEMISTRY B

Article

pubs.acs.org/JPCB

Depth-Dependent Membrane Ordering by Hemagglutinin Fusion Peptide Promotes Fusion

Hirak Chakraborty,*[,†,‡] Barry R. Lentz,*[,§] Mamata Kombrabail,[‖] G. Krishnamoorthy,[‖,⊥] and Amitabha Chattopadhyay*[,†]

[†]CSIR-Centre for Cellular and Molecular Biology, Uppal Road, Hyderabad 500 007, India

[‡]School of Chemistry, Sambalpur University, Jyoti Vihar, Burla, Odisha 768 019, India

[§]Department of Biochemistry and Biophysics and Program in Molecular and Cellular Biophysics, University of North Carolina at Chapel Hill, Chapel Hill, North Carolina, United States

[‖]Department of Chemical Sciences, Tata Institute of Fundamental Research, Homi Bhaba Road, Mumbai, India

Supporting Information

ABSTRACT: Membrane fusion, one of the most fundamental processes in life, occurs when two separate lipid membranes merge into a single continuous bilayer. Membrane fusion is essential for the entry of lipid-sheathed viruses such as influenza and HIV. Influenza virus is internalized via receptor-mediated endocytosis and then fuses with the endosomal membrane at low pH. Hemagglutinin, a glycoprotein found on the surface of influenza virus, is responsible for the fusion of the viral sheath with the endosomal membrane. The ∼20 amino acid long N-terminus of hemagglutinin, known as the fusion peptide, plays a crucial role in the viral fusion process. Although there exists vast literature on the importance and role of the fusion peptide in promoting membrane fusion, there is no consensus on the mechanism by which it promotes fusion. A recent report suggested that the fusion peptide occupies and orders space in the outer leaflets of contacting bilayers so as to promote acyl chain protrusion into interbilayer space and promote fusion "stalk" formation. We report here the effect of the wild type, G1S, G1V, and W14A mutants of hemagglutinin fusion peptide on depth-dependent ordering of model membranes along the bilayer normal. We utilized fluorescence anisotropy, lifetime measurements, and lifetime distribution analyses of different anthroyloxy stearic acid probes (*n*-AS) in order to examine the effect of fusion peptides at various depths along the bilayer normal. Wild type peptide uniquely ordered a region ∼12 Å from the bilayer midpoint, W14A and G1S mutants mainly ordered the bilayer interface, while G1V had little ordering influence. On the basis of recent analysis of the effects of these peptides on fusion, ordering of the mid-upper region of the bilayer appears to promote fusion pore formation, while ordering of the bilayer interface inhibits it.

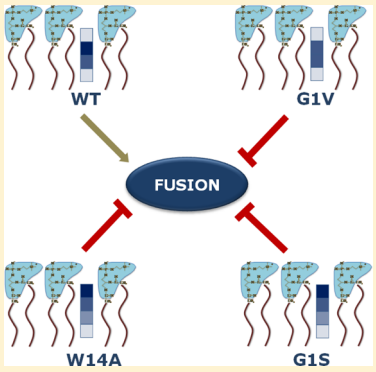

INTRODUCTION

Enveloped viruses enter cells via membrane fusion.[1] Some viruses fuse with the plasma membrane at the cell surface,[2,3] and others are first taken into cells by receptor-mediated endocytosis and subsequently fuse with the endosome.[4,5] The fusion process is triggered by either receptor binding (as in the entry of HIV) or low pH that prevails in the endosome (as in the case of influenza). The major glycoprotein on the influenza virus is initially synthesized as a precursor polypeptide, HA0, which is activated upon cleavage into two subunits, HA1 and HA2. HA1 is mainly responsible for receptor binding, while HA2 mediates fusion between the viral envelope and cellular membranes.[6,7] HA1 contains sialic acid binding sites that bind to the sialic acid which is present on the cell surface of its target cells. This causes the virus particle to stick to the cell surface.[5] Upon exposure to low pH (∼5.3), HA2 undergoes considerable conformational change leading to exposure of its glycine-rich N-terminal regions.[8,9] Mutations in a stretch of ∼20−25 amino acids in the N-terminal region of HA2 have been shown to block fusion-mediated viral infection, leading to this stretch of amino acids being termed "fusion peptide".[10]

The mechanism by which N-terminal fusion peptides promote fusion is not clear, although several putative mechanisms have been proposed.[11−21] It has been suggested that fusion peptides could promote membrane fusion by changing bending modulus,[20] filling void volume within intermediate nonbilayer structures,[16] providing a positive[11] or negative[22] intrinsic curvature to contacting bilayer leaflets, and reducing Gaussian energy.[18] Hemagglutinin (HA) fusion peptide is one of the most well studied fusion peptides. HA containing the wild type fusion peptide promotes both "hemifusion" and "fusion pore" between COS7 cell and labeled RBCs,[23] but HA with a G1S mutation allows only "hemifusion" in this assay, while G1V and W14A mutations block both processes.[23,24] A detailed kinetic study of poly(ethylene glycol)-

Received: January 21, 2017
Published: January 26, 2017

DOI: 10.1021/acs.jpcb.7b00684
J. Phys. Chem. B 2017, 121, 1640−1648

induced fusion of small unilamellar vesicles (SUVs) reveals that binding of all three mutant peptides permits intermediate formation but inhibits full fusion (pore formation), with G1V blocking it entirely, roughly in alignment with cell-based studies.[11] Possible mechanistic interpretations of these effects have been proposed on the basis of NMR- and ESR-based structures of fusion peptides attached to polylysine host peptides that are solubilized by dodecylphosphocholine (DPC) micelles[24−26] and peptide influences on bilayer structure.[11] X-ray diffraction study suggests that negative Gaussian curvature (a combination of positive and negative curvature in orthogonal directions) imparted by the wild type peptide (as opposed to mutant peptides) is associated with its ability to locate deeper into the bilayer and stabilize the pore-like cubic phase.[19] Spin-labeled lipid probes provide a different view and an opposing hypothesis for how wild type fusion peptides of either HA or the gp41 protein of HIV might promote fusion, namely, by ordering the headgroup region and promoting negative intrinsic curvature.[22,24,27] However, ordering at the membrane interface is not clearly correlated with fusogenic ability according to previously carried out studies using fluorescent probes like DPH, TMA-DPA, and C_6-NBDPC.[11,13,28] This indicates that the peptide-induced ordering at a particular location of the bilayer is critical to its fusion catalyzing ability, while which region of the bilayer is of importance remains poorly understood.

In this work, we explore the relationship between depth-dependent membrane perturbations induced by fusion peptides and their fusogenic efficiency. In order to define the effect of the fusion peptides better at various depths in the membrane, we employed steady state and time-resolved fluorescence spectroscopy using a series of depth-dependent fluorescent probes in model membranes. For this, we utilized *n*-anthroyloxy stearic acids (*n*-AS), in which an anthroyloxy group is attached at various positions of the alkyl chain. Anthroyloxy fatty acid probes represent a unique set of reporter molecules for parameters related to membrane penetration depth.[29] These probes have been found to be located at a graded series of depths in the membrane bilayer, depending on the position of the attachment of the anthroyloxy group to the fatty acyl chain[30−34] (see Figure S1). Thus, the distance of the anthroyloxy group from the bilayer center is established to be almost linearly related to the number of carbon atoms between the anthroyloxy and carboxyl groups.[31] Since all of the peptides examined here have comparable affinity ($K_d \sim 0.5\ \mu M$) for model membranes,[11] differences in peptide-induced changes in fluorescence anisotropy for a particular *n*-AS probe indicate a preferential depth-dependent membrane ordering property of the peptide. The change in fluorescence anisotropy for a particular *n*-AS probe will be enhanced if the peptide alters the membrane ordering at the depth where the particular *n*-AS probe is located. The effect of peptide at various depths was measured by calculating the initial slope of the anisotropy versus peptide concentration plot. The higher slope indicates the ability of the peptide to alter membrane ordering at a lower concentration.

Fluorescence lifetime is sensitive to local probe environment, and this is also true for *n*-AS probes.[32] We applied maximum entropy method (MEM) analysis of real time decay of fluorescence intensity in response to picosecond excitation to obtain lifetime distributions of *n*-AS probes in the absence and presence of the four HA fusion peptides considered here. Our results provide insight into the effects of peptides on the local environment at different depths within the bilayer. Taken together, these results provide a detailed depth-dependent insight about the effect of the wild type and mutant fusion peptides on the membrane in the context of membrane fusion. We propose that the depth-dependent membrane ordering profile induced by fusion peptides could be an important determinant in their fusogenic efficiency and provide a model correlating them.

EXPERIMENTAL SECTION

Materials. 1-Palmitoyl-2-oleoyl-*sn*-glycero-3-phosphocholine (POPC) was purchased from Avanti Polar Lipids (Alabaster, AL). 1,2-Dimyristoyl-*sn*-glycero-3-phosphocholine (DMPC) was obtained from Sigma Chemical Co. (St. Louis, MO). 2-, 6-, 9-, and 12-AS were purchased from Molecular Probes/Invitrogen (Eugene, OR). POPC was checked for purity by thin-layer chromatography on silica gel precoated plates (Sigma) in chloroform/methanol/water (65:35:5, v/v/v), and was found to give one spot with a phosphate-sensitive spray and on subsequent charring.[35] The concentration of POPC was determined by phosphate assay after total digestion by perchloric acid.[36] DMPC was used as an internal standard to assess the completeness of lipid digestion. Concentrations of stock solutions of *n*-AS probes in methanol were estimated using the molar extinction coefficient (ε) of 8000 M^{-1} cm^{-1} at 361 nm.[37] Solvents used were of spectroscopic grade, and purified water through a Millipore (Bedford, MA) Milli-Q system was used throughout.

Preparation of Hemagglutinin Peptides. The hemagglutinin peptides (native and mutants) were chemically synthesized by the solid phase method using fMOC chemistry and purified by high performance liquid chromatography. The sequences of the peptides are GLFGAIAGFIENGWEGMIDG (wild type), **S**LFGAIAGFIENGWEGMIDG (G1S mutant), **V**LFGAIAGFIENGWEGMIDG (G1V mutant), and GLFGAIAGFIENG**A**EGMIDG (W14A). A detailed description of the synthesis and purification of the wild type peptide is available elsewhere.[11] Stock peptide solutions were prepared in DMSO, and small aliquots of stock solutions were added to vesicle suspensions. The amount of DMSO was always less than 1% (v/v), and control experiments showed that this amount of DMSO had no detectable effect on membrane structure.

Preparation of Vesicles. All experiments were performed using large unilamellar vesicles (LUVs) containing 1% (mol/mol) 2-, 6-, 9-, or 12-AS. The probe to lipid ratio (mol/mol) was fixed at 1/100 considering the fact that, at this probe concentration (1 mol %), probe-induced membrane perturbation is minimal.[29−34] In addition, control experiments showed that the phase transition temperature of phospholipids in model membranes remains invariant in the presence of 1 mol % *n*-AS probes (data not shown). Briefly, 640 nmol of POPC in chloroform was mixed with 6.4 nmol of *n*-AS probe in methanol. A few drops of chloroform were added and mixed well, and the samples were dried under a stream of nitrogen while being warmed gently (~35 °C). After further drying under a high vacuum for at least 3 h, 1.5 mL of buffer (10 mM sodium acetate, 150 mM sodium chloride, pH 5) was added, and each sample was vortexed for 3 min to disperse the lipid and hydrated for an hour at room temperature (~23 °C). LUVs with a diameter of 100 nm were prepared by the extrusion technique using an Avanti Mini-Extruder (Alabaster, AL) as previously described.[38,39] Background samples were prepared the same way except that the probes were omitted.

DOI: 10.1021/acs.jpcb.7b00684
J. Phys. Chem. B 2017, 121, 1640−1648

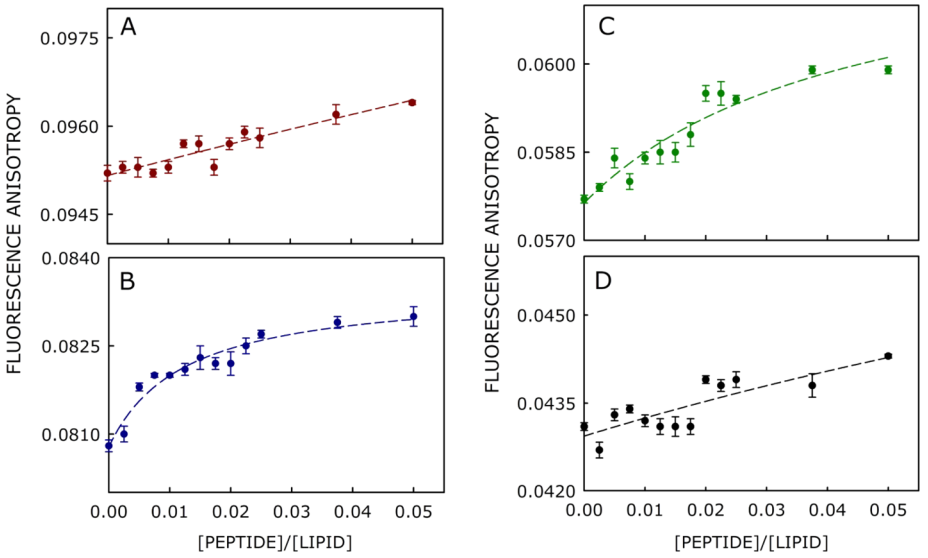

Figure 1. Depth-dependent ordering of the membrane along the bilayer normal induced by wild type peptide measured using *n*-AS probes. Steady state fluorescence anisotropy of (A) 2-AS, (B) 6-AS, (C) 9-AS, and (D) 12-AS with increasing concentration of fusion peptide in large unilamellar vesicles of POPC was measured to assess the depth-dependent ordering efficiency of wild type peptide. Data for parts B and C were fitted to the classical Langmuir model for adsorption of ligand to multiple, equivalent, and noninteracting surface sites. The straight lines illustrate the slopes of these curves at low surface occupancy. For parts A and D, straight lines provided an adequate description of the data. The ratio of probe to lipid was 1:100 (mol/mol), and the POPC concentration was 400 μM. Experiments were carried out at 23 °C and at pH 5. The excitation wavelength was 360 nm, and emission was monitored at 470 nm. The data represent means ± SE of at least three independent measurements. See the Experimental Section for other details.

Steady State Fluorescence Measurements. Steady state fluorescence measurements were performed at room temperature (~23 °C) with a Fluorolog-3 Model FL3-22 spectrofluorometer (Horiba Jobin Yvon, Edison, NJ), using a 1 cm path length quartz cuvette. Excitation and emission slits with a nominal band-pass of 3 nm were used for all measurements. Background (fluorophore-free) intensities of samples were subtracted from each sample spectrum to eliminate any contribution due to the solvent Raman peak and other scattering artifacts. Fluorescence anisotropy measurements were performed using the same instrument. Anisotropy values were calculated using the following equation[40]

$$r = \frac{I_{VV} - G \times I_{VH}}{I_{VV} + 2G \times I_{VH}} \quad (1)$$

where $G = I_{HV}/I_{HH,}$ (grating correction or *G*-factor) and I_{VV} and I_{VH} are the measured fluorescence intensities with the excitation polarizer vertically oriented and the emission polarizer vertically and horizontally oriented, respectively. All experiments were performed with multiple sets of samples, and average values of fluorescence anisotropy are shown in the figures.

Time-Resolved Fluorescence Measurements and Maximum Entropy Method (MEM) Analysis. Time-resolved fluorescence intensity decay measurements were carried out using a time-correlated single photon counting (TCSPC) setup as described earlier.[32] For fluorescence lifetime measurements, 1 ps pulses of 732 nm radiation from the Ti-sapphire femto/picosecond laser (Spectra Physics, Mountain View, CA), pumped by a Nd:YLF laser (Millenia X, Spectra Physics), were frequency-doubled to 366 nm by using a frequency doubler/tripler (GWU, Spectra Physics). Fluorescence emission of *n*-AS probes was measured at 470 nm using a combination of a monochromator and a 400 nm cutoff filter. Fluorescence intensity decay was collected from the sample after excitation with the emission polarizer oriented at the magic angle (54.7°) with respect to the excitation polarizer. To optimize the signal-to-noise ratio, 20,000 photons were collected in the peak channel. All experiments were performed using excitation and emission slits with a nominal bandpass of 3 nm or less. Data stored in the multichannel analyzer were routinely transferred to a computer for analysis. Fluorescence intensity decay curves so obtained were deconvoluted with the instrument response function and analyzed as a sum of exponential terms

$$F(t) = \sum_{i=1}^{N} \alpha_i \exp(-t/\tau_i) \quad (2)$$

where $F(t)$ is the fluorescence intensity at time t and α_i is a pre-exponential factor representing the fractional contribution to the time-resolved decay of the component with a lifetime τ_i such that $\sum_i \alpha_i = 1$. The decay parameters were recovered using a nonlinear least-squares iterative fitting procedure based on the Levenberg–Marquardt algorithm.[41,42] A fit was considered acceptable when plots of the weighted residuals and the autocorrelation function showed random deviation about zero with a minimum χ^2 value not more than 1.2. Both the discrete exponential analysis as well as the maximum entropy method (MEM) were used to analyze the fluorescence decays. In the MEM approach,[43,44] the fluorescence intensity decay ($F(t)$) is analyzed using the model of continuous distribution of lifetimes

$$F(t) = \int_0^\infty \alpha(\tau) \exp(-t/\tau)\, d\tau \quad (3)$$

where $\alpha(\tau)$ represents the amplitude corresponding to the lifetime τ in the intensity decay. The limits on this integration are generally set on the basis of the information regarding the specific system under study and the detection limit of the instrument. We set the lower and upper limits of the

DOI: 10.1021/acs.jpcb.7b00684
J. Phys. Chem. B 2017, 121, 1640−1648

integration as 10 ps and 10 ns, respectively. For practical reasons, this equation can also be written in terms of a discrete sum of exponentials as

$$F(t) = \sum_{i=1}^{N} \alpha_i \exp(-t/\tau_i) \quad (4)$$

where N represents the total number of exponentials. In our analysis, N is taken as 150 exponentials equally spaced in the $\log(\tau)$ space between the lower and upper limits. MEM initially starts with a flat distribution of amplitudes $\alpha(\tau)$, that is, assuming that each lifetime has equal contribution to the observed decay. The MEM arrives at the amplitude distribution that best describes the observed experimental fluorescence intensity decay. The optimization of the amplitude distribution $\alpha(\tau)$ is carried out in successive iterations by minimizing the χ^2 value (close to 1 in all cases) and maximizing the entropy (S).[45] The expression used for S is the Shannon−Jayne entropy function, expressed as $S = -\sum p_i \log p_i$, where $p_i = \alpha_i/\sum \alpha_i$. If the χ^2 criterion is satisfied by many distributions in a particular iteration, then the distribution with maximum entropy is selected. The analysis is terminated when χ^2 reaches the specified lower limit or when χ^2 and $\alpha(\tau)$ show no change in successive iterations. Importantly, MEM analysis gives a lifetime distribution that is robust and makes no assumption about the number of lifetime species (mean lifetimes in local distributions) that contribute to the data.[45,46]

RESULTS

Effect of Fusion Peptides on the Depth-Dependent Membrane Perturbation as Measured by Fluorescence Anisotropy of *n*-AS Probes. The effect of the wild type fusion peptide and its mutants on membrane structure was monitored along the bilayer normal using depth-dependent anthroyloxy probes attached at various positions of stearic acid. It has been previously shown that the anthroyloxy groups in *n*-AS probes are progressively localized at increasing depth as the site of attachment of the anthroyloxy group is moved from the 2- to the 12-position along an acyl chain,[31] thereby allowing the *n*-AS probes to act as membrane depth markers. We monitored the depth-dependent perturbation of the membrane, induced by increasing concentration of the wild type and mutant fusion peptides by measuring the fluorescence anisotropy of *n*-AS probes, which reflects the degree of probe mobility during its excited state lifetime. The fluorescence anisotropy of the probe will increase if the peptide induces ordering (increases packing due to its presence) at the vicinity of the probe. Figures 1 and S2−S4 show plots of fluorescence anisotropy as a function of peptide/lipid ratio for wild type and mutant peptides. The plots for 6-AS and 9-AS in Figure 1 appear to saturate, but those for 2-AS and 12-AS do not. This clearly indicates that the wild type peptide has minimum influence on the change in ordering near 2- and 12-AS. This difference correlates with the abilities of different probes to detect the ordering effects of peptides at various depths of the membrane. The saturating behavior was observed when peptide-induced membrane ordering efficiency is higher at a particular depth (6-AS and 9-AS for WT peptide), and roughly linear behavior was observed when ordering efficiency is minimal (2-AS and 12-AS for WT peptide). A smaller amount of the strongly perturbing peptide induces significant change in membrane ordering, and further addition does not induce additional membrane ordering. On the other hand, the influence of nonperturbing peptide is extremely small at lower concentration and shows considerable change only when a high concentration of peptide was added to the membrane. We have calculated the "initial slope" of the fluorescence anisotropy of *n*-AS probes vs [peptide]/[lipid] plots (Figure 1) and "change in magnitude of anisotropy" (Δr) to evaluate the effect of peptide on the ordering of the membrane environment (Table S1). The trends of "initial slope" and Δr values for *n*-AS probes are comparable in the presence of all four peptides (Table S1). For example, both Δr and "initial slope" display a higher value for 6- and 9-AS and a lower value for 2- and 12-AS in the presence of WT peptide. As "initial slope" and Δr values compare well, we have chosen "initial slope" to describe the effect of peptide on the membrane ordering at a particular depth. In addition, the change in "initial slope" is more robust as the magnitude of initial slope is larger than the Δr. The perturbing influences of different peptides therefore are well characterized in terms of the slopes of the curves in Figures 1 and S2−S4 at lower peptide/lipid ratios. These slopes are plotted in Figure 2 as a function of the distance from the bilayer midplane monitored by each probe[31] for each of the peptides examined here. The wild type peptide most severely orders the membrane at a distance of ∼11−12 Å from the bilayer midplane but retains some influence near 9 Å (Figure 2). A relatively small amount of WT peptide can induce considerable ordering in the upper region where its influence is the greatest. Similar plots of fluorescence anisotropy of *n*-AS probes in the presence of fusion-inefficient G1V, G1S, and W14A peptides (see Figures S2−S4) provide the other curves in Figure 2. The G1V peptide ordered the same region of the bilayer as WT peptide but to a somewhat lesser extent (Figure 2 and Figure S2). Similar to the WT peptide, G1V had almost no influence at the interface or near the bilayer midplane. The influences of G1S and W14A peptides on the bilayer order profile were very different from those of WT and G1V. Of all peptides, G1S had the largest ordering influence and its influence reached from the bilayer/water interface well into the bilayer interior, still being significant at the middle of the leaflet (Figure 2 and Figure

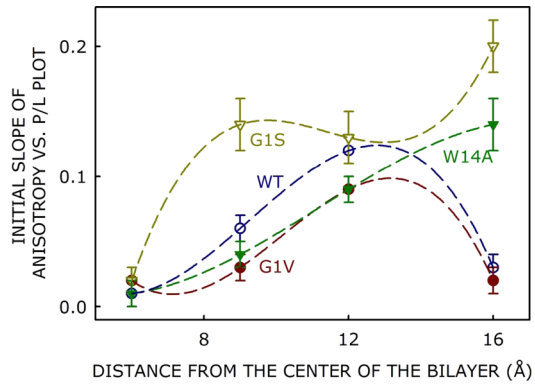

Figure 2. Effect of wild type and mutant fusion peptides on depth-dependent ordering of membranes along the bilayer normal. The efficiency of membrane ordering at various depths (Å), as obtained from the initial slopes of *n*-AS steady-state fluorescence anisotropy versus peptide/lipid ratio (e.g., as in Figure 1), is plotted versus the distance of the anthroyloxy group from the bilayer midplane (taken from ref 31). Data corresponding to results obtained with curves for different peptides are color-coded as in Figure 1, and the curves (derived from third-order polynomials) are meant only to guide the eye.

DOI: 10.1021/acs.jpcb.7b00684
J. Phys. Chem. B 2017, 121, 1640−1648

S3), where no other peptide had significant ordering influence. W14A peptide also had its greatest ordered effect at the interface, but unlike G1S, its influence did not extend as far into the leaflet, in which it was embedded (Figure 2 and Figure S4). The individual peptides produce a significantly different impact on *n*-AS anisotropy, as the inherent ability of a given peptide to order the bilayer at a particular depth is unique. The differential influence of the peptide at various depths could therefore be attributed to their difference in insertion depth and orientation in the membrane.

Effect of Fusion Peptides on Environmental Heterogeneity as Revealed by Fluorescence Lifetime Distributions. The full width at half-maximum (FWHM) of a fluorescence lifetime distribution reflects the environmental heterogeneity experienced by fluorophores during the excited state lifetime.[43,44,47] The width of the FWHM depends on the microenvironmental heterogeneity near the probe's location during its fluorescence lifetime and the rate $(1/\tau_S)$ at which the probe samples different microenvironments during its excited state lifetime.[47] Lipids diffuse laterally in a bilayer with $D^{(2)} \sim 10^{-8}$ cm^2 s^{-1},[48] and a probe diffusing similarly to a lipid would sample a lipid location with a cross-sectional area of ~70 Å^2 (i.e., a single lipid location) with $\tau_S \sim 200$ ns; i.e., it resides in a given environment sufficiently long for multiple excitation/emission events for an *n*-AS probe with a fluorescence lifetime of ~10 ns. In this instance, the fluorescence lifetime distribution will largely reflect the microscopic heterogeneity of probe locations in a bilayer. Thus, a smaller FWHM reflects decreased heterogeneity of microenvironments.

The FWHM of the fluorescence lifetime distribution of *n*-AS in fluid membrane bilayers varies considerably with "*n*": FWHM of 12-AS $\lesssim$ 9-AS $\lesssim$ 6-AS $\ll$ 2-AS.[32] Acyl chains in a fluid bilayer are increasingly disordered nearer to the bilayer center, so if the density of local hydrophobic microstructures were responsible for the variation of FWHM with distance from the bilayer center, FWHM should vary as 12-AS > 9-AS > 6-AS > 2-AS. The fact that this is opposite from our observation suggests that the FWHM must reflect the uniqueness of probe microstates in its microenvironment. The fluorophore in 2-AS is located at the membrane interface, in which polar interactions should occur between the probe excited state and both water and polar headgroups. This region therefore presents a variety of microenvironments and a large number of unique microstates, explaining the very large FWHM of this probe.[32] Since water molecules are widely recognized to enter the bilayer in small numbers,[49−52] it is reasonable to presume that lower "*n*" corresponds to the increased presence of polar water in regions closer to the bilayer interface and further from the hydrophobic center.[32]

Figure 3 shows the representative lifetime distribution of 6-AS in POPC membranes in the absence and presence of the wild type and G1S, G1V, and W14A mutant fusion peptides. The distribution is bimodal with peaks centered at 5−7 and ~12 ns due to emission from two distinct excited state conformations. The unstable ground-state conformation consists of a nonplanar arrangement of the carboxy and anthrancene groups, while a relaxed excited state conformation permits a roughly planar arrangement.[53] The FWHM of 6-AS lifetime distributions in the presence of the wild type peptide is remarkably narrow relative to the FWHM in the peptide-free bilayer or in the presence of mutant peptides. Another remarkable feature is that the mean lifetime of the stable excited state conformation remains constant at ~12 ns in

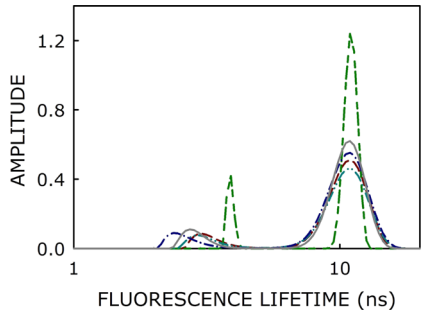

Figure 3. MEM lifetime distribution of 6-AS in POPC membranes in the absence of any peptide (gray, —) and in the presence of wild type (green, — –), G1S (maroon, — —), G1V (blue, — · —), and W14A (cyan, — · · —) peptides. All other conditions are as in Figure 1. See the Experimental Section for other details.

peptide-free and peptide-containing bilayers. Parts A−C in Figure 4 summarize the FWHM values for 2-, 6-, and 9-AS probes for the wild type and mutant fusion peptides. The lifetime measurements were not carried out with 12-AS, since no peptide-induced change was observed in fluorescence anisotropy measurements for 12-AS (see Figure 2).

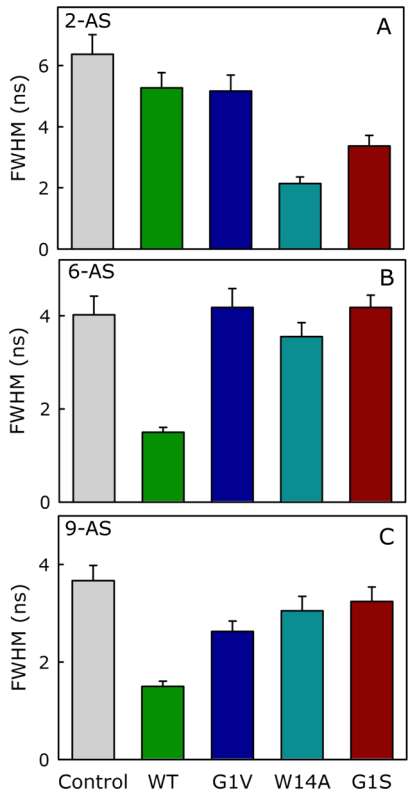

Figure 4. Environmental heterogeneity, as detected by lifetime distribution analysis, is altered by the wild type and mutant fusion peptides differentially at varying depths of POPC membranes. The full width at half maxima (FWHM) of the fluorescence lifetime distribution of (A) 2-AS, (B) 6-AS, and (C) 9-AS are plotted for the absence of any peptide (gray) and in the presence of wild type (green), G1V (blue), W14A (cyan), and G1S (maroon). All other conditions are as in Figure 1. Data represent means ± SE of at least three independent measurements. See the Experimental Section for other details.

DOI: 10.1021/acs.jpcb.7b00684
J. Phys. Chem. B 2017, 121, 1640−1648

DISCUSSION

Kinetic studies[11] as well as molecular dynamics simulations[54,55] of peptide-induced membrane fusion suggest that the wild type HA fusion peptide catalyzes the "stalk formation" by filling space in the hydrophobic region of the exposed bilayer leaflet and thus promote acyl chain excursion into the dehydrated interbilayer space. The tentative structure of wild type and mutant peptide on membranes was proposed from NMR and ESR studies performed with fusion peptides attached to a polylysine host peptide at their C-terminus and solubilized in DPC micelles.[24−26] The current study provides additional information on the perturbation at various depth positions along the bilayer normal induced by the wild type and mutant peptides.

Insights into Peptide Location, Motions, and Structure. Our results with *n*-AS probes provide precise information about the peptide influence on bilayer structure at different locations along the bilayer normal. The surface occupied by each peptide is approximately the same (similar K_d); the variation of the fluorescence anisotropy of *n*-AS with peptide to lipid ratio (Figure 2) reflects the inherent ability of a given peptide to order the bilayer at the particular depth at which the anthroyloxy probe is located in the membrane.

In addition to fluorescence anisotropy, we use the FWHM of the fluorescence lifetime distribution as a measure of environmental heterogeneity that appears to reflect water penetration to the depth of the anthroyloxy probe, with increased FWHM indicating increased water penetration at the probe surroundings. Our results indicate that the WT peptide maximally orders the bilayer at 10−14 Å from the center of the bilayer (as detected by the 6-AS probe), and somewhat orders slightly below the midpoint of the outer leaflet (8−10 Å, 9-AS probe). Its influence rapidly dissipates above this region, as indicated by minimal ordering detected by the 2-AS probe (Figure 2). Chain ordering by WT peptide is accompanied by significant exclusion of water (Figure 4B and C). These results indicate that the WT peptide occupies significant space and aligns with acyl chains at and somewhat below the midpoint of the outer leaflet of the membrane. Taken together, our results show that wild type HA fusion peptide occupies space, excludes water, and orders the mid region of the outer leaflet about 10−14 Å from the bilayer center.

Figure 2 points out that the G1V peptide orders a region of the membrane that is also ordered by WT peptide (10−14 Å from the bilayer mid plane, 6-AS probe), but the extent of ordering is smaller than the WT peptide. In addition, GIV peptide fails to exclude water from the region (Figure 4), which is unlike the WT peptide. It clearly excludes water deeper into the bilayer (9-AS probe) (Figure 4) and slightly disorders this region (Figure 2). Thus, while the Val of the G1V peptide appears to occupy space in the upper region of the bilayer, it does not intercalate well between acyl chains and fails to exclude water.

NMR studies of a host−guest 20-residue W14A peptide in DPC micelles suggest that the peptide has a very broad conformational distribution, making it difficult to locate the peptide in the bilayer.[24] W14A does not order the middle of the exposed bilayer leaflet (Figure 2) but orders the 2-AS probe (Figure 2) and excludes water from this probe environment (Figure 4). This suggests that W14A is located within the bilayer interface and it explores the region just below the interface. Loss of Trp14 also means that it is unlikely to be tightly anchored to the interface, as are the other peptides examined.

A model based on NMR and ESR data shows the G1S peptide is having an overall conformation in the bilayer that is quite similar to that of WT peptide.[56] Like W14A, G1S orders (Figure 2) and excludes water (Figure 4) from the bilayer interface. Unlike W14A, G1S also significantly orders the 9-AS probe near the bilayer center (Figure 2), something even WT peptide did not do. At the same time, it did not reduce the FWHM of the 6-AS probe and only slightly sharpened that of the 9-AS probe. This anomalous behavior suggests that G1S behaves very differently from WT peptide. While a broad lifetime distribution can indicate water penetration, also the Ser of G1S could impart some polarity near the probe (9-AS) and influence its lifetime distribution. This would be consistent with the structure proposed on the basis of NMR and ESR data.[56] However, a Ser located deep in the bilayer nonpolar core would be thermodynamically unfavorable and would likely be drawn toward the polar membrane interface. This would account for the significant ordering (Figure 2) and narrow lifetime distribution (Figure 4) of the 2-AS probe. Thus, our results suggest that the G1S peptide distributes between interface-located and inserted configurations.

Implications for Membrane Fusion. It is widely recognized that membrane fusion is a multistep process with formation of an initial "hemifusion" intermediate and evolution of this either to direct "fusion pore" formation or fusion pore formation through another intermediate.[16,57,58] The peptides examined here have a different effect on the different steps of the membrane fusion process. The difference in their effect might be attributed to their differential location and dynamic structures in the lipid bilayer. Incidentally, all of the peptides promote the initial "hemifusion" formation[11] and that could be due to the properties of the peptides to order and limit water penetration in the upper region of the bilayer, which could in turn help to stabilize the transition state of the initial "hemifusion" formation by facilitating the acyl chain protrusion into the interbilayer space. Our results indicate that the depth-dependent ordering information on the membrane may not be crucial for the "hemifusion" intermediate formation. We will therefore focus our discussion mainly on the effect of differential depth-dependent ordering of the membrane on the "pore-formation" step in the presence of WT and mutant peptides.

Implications for Fusion Pore Formation. As noted, all peptides catalyzed the formation of the initial intermediate (stalk or hemifusion). Beyond this step, the initial stalk intermediate proceeds to a pore via a single-bilayer diaphragm surrounded by a highly stressed edge having "Gaussian curvature" (positive and negative in different orthogonal directions on a surface).[18] The WT fusion peptide significantly increases the extent of fusion pore formation and induces pore formation in the early phase of the fusion process.[11] The ability of WT peptide to order acyl chains and exclude water in the upper region of the bilayer (Figures 2 and 4) gives it a positive "intrinsic" curvature that should destabilize the net negatively curved diaphragm edge and promote transient leakage of trapped contents across the diaphragm, to account for increased "content mixing" early in the fusion process.

In contrast, the mutant G1V, G1S, and W14A peptides all reduced the extent of pore formation but in different ways.[11] The G1V peptide showed the unique ability to order but admit water into the upper bilayer while disordering the middle

DOI: 10.1021/acs.jpcb.7b00684
J. Phys. Chem. B 2017, 121, 1640−1648

bilayer (Figures 2 and 4). It also uniquely blocked pore formation but dramatically increased content leakage.[11] Taken together, these results support previous speculation that a flexible G1V configuration could allow the bulky valine to occupy the interface, thereby entropically stabilizing the initial intermediate state at high temperatures, to the extent that the latter intermediates rupture and no longer form a fusion pore. Very little was directly known about the bilayer location or structural influence of G1S peptide, although it was speculated to contribute an intrinsic negative curvature. This seems unlikely based on the current results (Figures 2 and 4). The unusual behavior of G1S peptide demonstrated here is that it increases bilayer order and inhibits water penetration both at and below the interface, suggesting a flexible distribution between surface-located and buried conformations. G1S inhibits content mixing largely by dramatically reducing it at lower temperatures in the first and second intermediate states,[11] wherein content mixing is attributed to transient pores.[57,58] On the basis of our results, we suggest that the ability of G1S peptide to occupy different bilayer regions would permit it to accommodate and stabilize the unfavorable nonbilayer edge of the diaphragm-like intermediates. This would account for reduced content mixing and leakage in these intermediate states in the presence of G1S but would still permit expansion of diaphragm-like intermediates into a stable fusion pore, as reported.[11] Like G1S, the location of W14A in the bilayer was not well-defined, but it is speculated to contribute intrinsic negative curvature.[11] On the contrary, W14A peptide behaves similarly to G1S except that it seems to lack the flexibility that allows G1S to order chains near the bilayer center (Figures 2 and 4). This explains its inability to limit content mixing and leakage in the diaphragm intermediates that is observed for G1S peptide.

In summary, we report here a comparative depth-dependent effect of wild type and mutant HA fusion peptides on the membrane along the bilayer normal. Our results suggest a correlation between depth-dependent membrane ordering and the fusogenic property of the peptides.

■ ASSOCIATED CONTENT

Supporting Information

The Supporting Information is available free of charge on the ACS Publications website at DOI: 10.1021/acs.jpcb.7b00684.

Figure S1, a schematic representation of half of the membrane bilayer showing the localizations of the anthroyloxy groups in *n*-AS probes; Figures S2−S4, the depth-dependent ordering of the membrane along the bilayer normal induced by G1V, G1S, and W14A mutant peptides measured using *n*-AS probes; Table S1, the Δr and "initial slopes" calculated from Figure 1 and Figures S2−S4 for *n*-AS probes in the presence of WT, G1V, G1S, and W14 peptides (PDF)

■ AUTHOR INFORMATION

Corresponding Authors

*E-mail: hirakchakraborty@gmail.com. Phone: +91-8008716419.

*E-mail: uncbrl@med.unc.edu. Phone: 919-966-5384.

*E-mail: amit@ccmb.res.in. Phone: +91-40-2716-0059.

ORCID

Hirak Chakraborty: 0000-0001-7499-5707

Amitabha Chattopadhyay: 0000-0002-2618-2565

Present Address

⊥G.K.: Department of Biotechnology, Anna University, Chennai 600 025, India.

Notes

The authors declare no competing financial interest.

■ ACKNOWLEDGMENTS

This work was supported by research grants from the Council of Scientific and Industrial Research (A.C.) and Department of Atomic Energy (G.K.), Govt. of India, and NIH grant GM32707 (B.R.L.). A.C. and G.K. gratefully acknowledge support from J.C. Bose Fellowship (Department of Science and Technology, Govt. of India). H.C. thanks the Council of Scientific and Industrial Research (Govt. of India) for the award of a Senior Research Associateship and the University Grants Commission for UGC-Assistant Professor position and UGC-Start-Up Grant (F.4-5(138-FRP)/2014(BSR)). A.C. is an Adjunct Professor of Tata Institute of Fundamental Research (Mumbai), RMIT University (Melbourne, Australia), Indian Institute of Technology (Kanpur), and Indian Institute of Science Education and Research (Mohali). We thank G. Aditya Kumar for help in making figures and members of the Chattopadhyay laboratory for their comments and suggestions.

■ REFERENCES

(1) Hughson, F. M. Enveloped Viruses: A Common Mode of Membrane fusion? *Curr. Biol.* **1997**, *7*, 565−569.

(2) Dimitrov, D. S.; Golding, H.; Blumenthal, R. Initial Stages of HIV-1 Envelope Glycoprotein-mediated Cell Fusion Monitored by a New Assay Based on Redistribution of Fluorescent Dyes. *AIDS Res. Hum. Retroviruses* **1991**, *7*, 799−805.

(3) Freed, E. O.; Myers, D. J.; Risser, R. Characterization of the Fusion Domain of the Human Immunodeficiency Virus Type 1 Envelope Glycoprotein gp41. *Proc. Natl. Acad. Sci. U. S. A.* **1990**, *87*, 4650−4654.

(4) Earp, L. J.; Delos, S. E.; Park, H. E.; White, J. M. The Many Mechanisms of Viral Membrane Fusion Proteins. *Curr. Top. Microbiol. Immunol.* **2005**, *285*, 25−66.

(5) Skehel, J. J.; Wiley, D. C. Receptor Binding and Membrane Fusion in Virus Entry: the Influenza Hemagglutinin. *Annu. Rev. Biochem.* **2000**, *69*, 531−569.

(6) Prabhu, N.; Prabakaran, M. H.; Ho, T.; Velumani, S.; Qiang, J.; Goutama, M.; Kwang, J. Monoclonal Antibodies Against the Fusion Peptide of Hemagglutinin Protect Mice from Lethal Influenza A Virus H5N1 Infection. *J. Virol.* **2009**, *83*, 2553−2562.

(7) Stevens, J.; Blixt, O.; Tumpey, T. M.; Taubenberger, J. K.; Paulson, J. C.; Wilson, I. A. Structure and Receptor Specificity of the Hemagglutinin from an H5N1 Influenza Virus. *Science* **2006**, *312*, 404−410.

(8) Durell, S. R.; Martin, I.; Ruysschaert, J. M.; Shai, Y.; Blumenthal, R. What Studies of Fusion Peptides Tell Us About Viral Envelope Glycoprotein-mediated Membrane Fusion? *Mol. Membr. Biol.* **1997**, *14*, 97−112.

(9) White, J. M. Viral and Cellular Membrane Fusion Proteins. *Annu. Rev. Physiol.* **1990**, *52*, 675−697.

(10) Gething, M. J.; Doms, R. W.; York, D.; White, J. Studies on the Mechanism of Membrane Fusion: Site-specific Mutagenesis of the Hemagglutinin of Influenza Virus. *J. Cell Biol.* **1986**, *102*, 11−23.

(11) Chakraborty, H.; Tarafdar, P. K.; Klapper, D. G.; Lentz, B. R. Wild-type and Mutant Hemagglutinin Fusion Peptides Alter Bilayer Structure as well as Kinetics and Activation Thermodynamics of Stalk and Pore Formation Differently: Mechanistic Implications. *Biophys. J.* **2013**, *105*, 2495−2506.

(12) Epand, R. F.; Martin, I.; Ruysschaert, J. M.; Epand, R. M. Membrane Orientation of the SIV Fusion Peptide Determines its

DOI: 10.1021/acs.jpcb.7b00684
J. Phys. Chem. B 2017, 121, 1640−1648

Effect on Bilayer Stability and Ability to Promote Membrane Fusion. *Biochem. Biophys. Res. Commun.* **1994**, *205*, 1938−1943.
(13) Haque, M. E.; Chakraborty, H.; Koklic, T.; Komatsu, H.; Axelsen, P. H.; Lentz, B. R. Hemagglutinin Fusion Peptide Mutants in Model Membranes: Structural Properties, Membrane Physical Properties, and PEG-mediated Fusion. *Biophys. J.* **2011**, *101*, 1095−1104.
(14) Kozlovsky, Y.; Kozlov, M. M. Stalk Model of Membrane Fusion: Solution of Energy Crisis. *Biophys. J.* **2002**, *82*, 882−895.
(15) Larsson, P.; Kasson, P. M. Lipid Tail Protrusion in Simulations Predicts Fusogenic Activity of Influenza Fusion Peptide Mutants and Conformational Models. *PLoS Comput. Biol.* **2013**, *9*, e1002950.
(16) Malinin, V. S.; Lentz, B. R. Energetics of Vesicle Fusion Intermediates: Comparison of Calculations with Observed Effects of Osmotic and Curvature Stresses. *Biophys. J.* **2004**, *86*, 2951−2964.
(17) Siegel, D. P. The Modified Stalk Mechanism of Lamellar/Inverted Phase Transitions and its Implications for Membrane Fusion. *Biophys. J.* **1999**, *76*, 291−313.
(18) Siegel, D. P. The Gaussian Curvature Elastic Energy of Intermediates in Membrane Fusion. *Biophys. J.* **2008**, *95*, 5200−5215.
(19) Tenchov, B. G.; MacDonald, R. C.; Lentz, B. R. Fusion Peptides Promote Formation of Bilayer Cubic Phases in Lipid Dispersions. An X-ray Diffraction Study. *Biophys. J.* **2013**, *104*, 1029−1037.
(20) Tristram-Nagle, S.; Nagle, J. F. HIV-1 Fusion Peptide Decreases Bending Energy and Promotes Curved Fusion Intermediates. *Biophys. J.* **2007**, *93*, 2048−2055.
(21) Zemel, A.; Ben-Shaul, A.; May, S. Modulation of the Spontaneous Curvature and Bending Rigidity of Lipid Membranes by Interfacially Adsorbed Amphipathic Peptides. *J. Phys. Chem. B* **2008**, *112*, 6988−6996.
(22) Ge, M.; Freed, J. H. Fusion Peptide from Influenza Hemagglutinin Increases Membrane Surface Order: an Electron-Spin Resonance Study. *Biophys. J.* **2009**, *96*, 4925−4934.
(23) Qiao, H.; Armstrong, R. T.; Melikyan, G. B.; Cohen, F. S.; White, J. M. A Specific Point Mutant at Position 1 of the Influenza Hemagglutinin Fusion Peptide Displays a Hemifusion Phenotype. *Mol. Biol. Cell* **1999**, *10*, 2759−2769.
(24) Lai, A. L.; Park, H.; White, J. M.; Tamm, L. K. Fusion Peptide of Influenza Hemagglutinin Requires a Fixed Angle Boomerang Structure for Activity. *J. Biol. Chem.* **2006**, *281*, 5760−5770.
(25) Han, X.; Bushweller, J. H.; Cafiso, D. S.; Tamm, L. K. Membrane Structure and Fusion-Triggering Conformational Change of the Fusion Domain from Influenza Hemagglutinin. *Nat. Struct. Biol.* **2001**, *8*, 715−720.
(26) Li, Y.; Tamm, L. K. Structure and Plasticity of the Human Immunodeficiency Virus gp41 Fusion Domain in Lipid Micelles and Bilayers. *Biophys. J.* **2007**, *93*, 876−885.
(27) Lai, A. L.; Freed, J. H. HIV gp41 Fusion Peptide Increases Membrane Ordering in a Cholesterol-Dependent Fashion. *Biophys. J.* **2014**, *106*, 172−181.
(28) Haque, M. E.; Koppaka, V.; Axelsen, P. H.; Lentz, B. R. Properties and Structures of the Influenza and HIV Fusion Peptides on Lipid Membranes: Implications for a Role in Fusion. *Biophys. J.* **2005**, *89*, 3183−3194.
(29) Chattopadhyay, A.; Mukherjee, S. Depth-Dependent Solvent Relaxation in Membranes: Wavelength-Selective Fluorescence as a Membrane Dipstick. *Langmuir* **1999**, *15*, 2142−2148.
(30) Abrams, F. S.; Chattopadhyay, A.; London, E. Determination of the Location of Fluorescent Probes Attached to Fatty Acids Using Parallax Analysis of Fluorescence Quenching: Effect of Carboxyl Ionization State and Environment on Depth. *Biochemistry* **1992**, *31*, 5322−5327.
(31) Abrams, F. S.; London, E. Extension of the Parallax Analysis of Membrane Penetration Depth to the Polar Region of Model Membranes: Use of Fluorescence Quenching by a Spin-Label Attached to the Phospholipid Polar Headgroup. *Biochemistry* **1993**, *32*, 10826−10831.
(32) Haldar, S.; Kombrabail, M.; Krishnamoorthy, G.; Chattopadhyay, A. Depth-Dependent Heterogeneity in Membranes by Fluorescence Lifetime Distribution Analysis. *J. Phys. Chem. Lett.* **2012**, *3*, 2676−2681.
(33) Villalaín, J.; Prieto, M. Location and Interaction of N-(9-anthroyloxy)-Stearic Acid Probes Incorporated in Phosphatidylcholine Vesicles. *Chem. Phys. Lipids* **1991**, *59*, 9−16.
(34) Chakraborty, H.; Haldar, S.; Chong, P. L.; Kombrabail, M.; Krishnamoorthy, G.; Chattopadhyay, A. Depth-Dependent Organization and Dynamics of Archaeal and Eukaryotic Membranes: Development of Membrane Anisotropy Gradient with Natural Evolution. *Langmuir* **2015**, *31*, 11591−11597.
(35) Baron, C. B.; Coburn, R. F. Comparison of Two Copper Reagents for Detection of Saturated and Unsaturated Neutral Lipids by Charring Densitometry. *J. Liq. Chromatogr.* **1984**, *7*, 2793−2801.
(36) McClare, C. W. An Accurate and Convenient Organic Phosphorus Assay. *Anal. Biochem.* **1971**, *39*, 527−530.
(37) Haugland, R. P. *Handbook of Fluorescent Probes and Research Chemicals*; Molecular Probes Inc.: Eugene, OR, 1996.
(38) MacDonald, R. C.; MacDonald, R. I.; Menco, B. P.; Takeshita, K.; Subbarao, N. K.; Hu, L. R. Small-Volume Extrusion Apparatus for Preparation of Large, Unilamellar Vesicles. *Biochim. Biophys. Acta, Biomembr.* **1991**, *1061*, 297−303.
(39) Mukherjee, S.; Chattopadhyay, A. Influence of Ester and Ether Linkage in Phospholipids on the Environment and Dynamics of the Membrane Interface: a Wavelength-Selective Fluorescence Approach. *Langmuir* **2005**, *21*, 287−293.
(40) Lakowicz, J. R. *Principles of Fluorescence Spectroscopy*; Plenum Press: New York, 1983.
(41) Bevington, P. R. *Data Reduction and Error Analysis for the Physical Sciences*; McGraw-Hill: New York, 1969.
(42) O'Connor, D. V.; Phillips, D. *Time-Correlated Single Photon Counting*; Academic Press: London, 1984.
(43) Haldar, S.; Kombrabail, M.; Krishnamoorthy, G.; Chattopadhyay, A. Monitoring Membrane Protein Conformational Heterogeneity by Fluorescence Lifetime Distribution Analysis Using the Maximum Entropy Method. *J. Fluoresc.* **2010**, *20*, 407−413.
(44) Mukherjee, S.; Kombrabail, M.; Krishnamoorthy, G.; Chattopadhyay, A. Dynamics and Heterogeneity of Bovine Hippocampal Membranes: Role of Cholesterol and Proteins. *Biochim. Biophys. Acta, Biomembr.* **2007**, *1768*, 2130−2144.
(45) Brochon, J. C. Maximum Entropy Method of Data Analysis in Time-Resolved Spectroscopy. *Methods Enzymol.* **1994**, *240*, 262−311.
(46) Swaminathan, R.; Krishnamoorthy, G.; Periasamy, N. Similarity of Fluorescence Lifetime Distributions for Single Tryptophan Proteins in the Random Coil State. *Biophys. J.* **1994**, *67*, 2013−2023.
(47) Krishnamoorthy, G.; Ira. Fluorescence Lifetime Distribution in Characterizing Membrane Microheterogeneity. *J. Fluoresc.* **2001**, *11*, 247−253.
(48) Jacobson, K.; Ishihara, A.; Inman, R. Lateral Diffusion of Proteins in Membranes. *Annu. Rev. Physiol.* **1987**, *49*, 163−175.
(49) Haines, T. H. Do Sterols Reduce Proton and Sodium Leaks through Lipid Bilayers? *Prog. Lipid Res.* **2001**, *40*, 299−324.
(50) Ira; Krishnamoorthy, G. Probing the Link Between Proton Transport and Water Content in Lipid Membranes. *J. Phys. Chem. B* **2001**, *105*, 1484−1488.
(51) Pandit, S. A.; Bostick, D.; Berkowitz, M. L. Mixed Bilayer Containing Dipalmitoylphosphatidylcholine and Dipalmitoylphosphatidylserine: Lipid Complexation, Ion Binding, and Electrostatics. *Biophys. J.* **2003**, *85*, 3120−3131.
(52) Ho, C.; Stubbs, C. D. Hydration at the Membrane Protein-Lipid Interface. *Biophys. J.* **1992**, *63*, 897−902.
(53) Berberan-Santos, M. N.; Prieto, M. J. E.; Szabo, A. G. Excited-State Intramolecular Relaxation of the Lipophilic Probe 12-(9-anthroyloxy)stearic Acid. *J. Phys. Chem.* **1991**, *95*, 5471−5475.
(54) Kasson, P. M.; Lindahl, E.; Pande, V. S. Atomic-Resolution Simulations Predict a Transition State for Vesicle Fusion Defined by Contact of a Few Lipid Tails. *PLoS Comput. Biol.* **2010**, *6*, e1000829.
(55) Smirnova, Y. G.; Marrink, S. J.; Lipowsky, R.; Knecht, V. Solvent-Exposed Tails as Prestalk Transition States for Membrane Fusion at Low Hydration. *J. Am. Chem. Soc.* **2010**, *132*, 6710−6718.

DOI: 10.1021/acs.jpcb.7b00684
J. Phys. Chem. B 2017, 121, 1640−1648

(56) Li, Y.; Han, X.; Lai, A. L.; Bushweller, J. H.; Cafiso, D. S.; Tamm, L. K. Membrane Structures of the Hemifusion-Inducing Fusion Peptide Mutant G1S and the Fusion-Blocking Mutant G1V of Influenza Virus Hemagglutinin Suggest a Mechanism for Pore Opening in Membrane Fusion. *J. Virol.* **2005**, *79*, 12065−12076.
(57) Chakraborty, H.; Tarafdar, P. K.; Bruno, M. J.; Sengupta, T.; Lentz, B. R. Activation Thermodynamics of Poly(ethylene glycol)-Mediated Model Membrane Fusion Support Mechanistic Models of Stalk and Pore Formation. *Biophys. J.* **2012**, *102*, 2751−2760.
(58) Weinreb, G.; Lentz, B. R. Analysis of Membrane Fusion as a Two-State Sequential Process: Evaluation of the Stalk Model. *Biophys. J.* **2007**, *92*, 4012−4029.

DOI: 10.1021/acs.jpcb.7b00684
J. Phys. Chem. B 2017, 121, 1640−1648